

High Active Material Loading in Organic Electrodes Enabled by an in-situ Electropolymerized π -Conjugated Tetrakis (4-Aminophenyl) Porphyrin

Thomas Smok,^[a, b] Ebrahim Abouzari-Lotf,^{*[a, b]} Sebastian Frentzen,^[a, b] Thomas Diemant,^[a] and Maximilian Fichtner^{*[a, b]}

Porphyrin complexes have been widely studied as promising electrode material in diverse energy storage systems and chemistries. However, like other organic electrodes, porphyrins often suffer from low conductivity and, consequently, require a significant amount (typically 40%) of electrochemically inactive conductive carbon that occupies volume and mass without storing energy. In this study, we investigate [5,10,15,20 tetrakis(4-aminophenyl)-porphyrin] (TAPP) and its metal complexes as redox-active cathode materials to address the aforementioned issues. The lithium-ion cells prepared with a high content of CuTAPP active material (70 wt %) demonstrate a stable discharge capacity of ~120 mAh/g when cycling with a

constant current density of 1000 mA/g. The material also showed superior rate capability, e.g., ~60 mAh/g at 8 A/g. The results of DFT calculations and experimental analysis indicate that the degree of planarity of the metalloporphyrins directly correlates to their cycling stability. Moreover, the contribution from the central metal redox during the cycling is found to be the reason for the significantly higher performance of the Cu-complex compared to the metal-free complex. The findings of this study show a general approach for facing common conductivity challenges of organic electrodes and open up a pathway for practical application of organics electrode materials in energy storage application.

Introduction

Research on organic electrode materials (OEMs) for rechargeable batteries has attracted high interest recently.^[1] The reasons for this development are some inherent features of organic electrode materials. Specifically, the facile variation of the redox-active functional groups, required for charge storage, gives easy access to a broad range of redox potentials and allows boosting storage capacity. Furthermore, OEMs may be synthesized from readily available organic precursors. In combination with improved recycling strategies,^[2] OEMs could limit the use of environmentally harmful, rare, and toxic heavy metals and become an alternative to inorganic compounds. Moreover, several reports have already indicated the intrinsic advantages of OEMs for post-lithium secondary batteries based

on multivalent shuttle ions as well as fast charging systems, since the type and extent of the interactions with ions could also be tuned.^[3]

Up to now, the use of various OEMs with diverse *n*- and *p*-type functionalities has been tested in rechargeable batteries.^[1a] However, practical applications have been often hampered due to some fundamental challenges of OEMs. The first challenge is a rapid decay in capacity due to instability and dissolution under charge-discharge processes in aprotic electrolytes. The second major issue, however, is the low conductivity of organic materials, which necessitates adding substantial amounts of conducting additives. This issue becomes evident when considering the achievable volumetric energy density with OEMs. Volumetric energy density is typically low, due to their intrinsic low volumetric mass densities^[1a] (below 2 g cm⁻³). Therefore, the development of OEMs with inherent conductivity may be an approach to mitigate or overcome the above-mentioned limitations. Besides such challenges, the performance of *n*-type OEMs has been frequently limited by low redox potential.^[4] For *p*-type organics, the main limitation is the small charge-storage capability.^[5] Using bipolar-type (*b*-type) OEMs was considered as a common strategy to improve the capacity and discharge voltage of OEMs compared to *p*- and *n*-type materials, respectively.^[4–6]

Tetrapyrrole macrocycles (TPMs, i.e., porphyrins, phthalocyanines, and related porphyrinoid analogs) are known as one of the most promising representatives of the material class of *b*-type electrodes.^[6,7] TPMs with aromatic $(4n+2)^{[8]}$ or antiaromatic $4n^{[6]}$ π -electron systems have been explored as OEMs. The small gap between the highest occupied molecular orbital (HOMO) and the lowest unoccupied molecular orbital (LUMO)

[a] T. Smok, Dr. E. Abouzari-Lotf, S. Frentzen, Dr. T. Diemant, Prof. Dr. M. Fichtner
Helmholtz Institute Ulm (HIU)
Helmholtzstraße 11,
89081 Ulm (Germany)

[b] T. Smok, Dr. E. Abouzari-Lotf, S. Frentzen, Prof. Dr. M. Fichtner
Institute of Nanotechnology
Karlsruhe Institute of Technology
P.O. Box 3640,
76021 Karlsruhe (Germany)
E-mail: ebrahim.abouzari-lotf@kit.edu
m.fichtner@kit.edu

 Supporting information for this article is available on the WWW under
<https://doi.org/10.1002/batt.202300026>

 © 2023 The Authors. Batteries & Supercaps published by Wiley-VCH GmbH. This is an open access article under the terms of the Creative Commons Attribution License, which permits use, distribution and reproduction in any medium, provided the original work is properly cited.

of the TPMs and the fact that the charges in the redox process will be stabilized in the mesomeric core enable high redox activities via fast electron uptake and release.^[7a] Facile redox of TPMs is well known, and complexes with promising redox behavior in diverse storage systems of Li,^[9] Na,^[10] K,^[11] Mg^[12] and Al^[13] were reported recently. To mitigate the undesired solubility of TPMs, researchers have either polymerized the active materials in advance^[14] or enabled polymerization in-situ during cycling.^[8a,11,15] Polymerization reaction that leads to the formation of π -conjugated linkages will enhance the electrical conductivity and reduce the HOMO-LUMO gap of the material, allowing faster redox processes.^[15a]

For the well-known copper-porphyrin complex (CuDEPP),^[8a] storage of four electrons corresponds to a specific capacity of 187 mAh/g. An average discharge voltage of 3.0 V was observed, at an active material ratio of 50% in the electrode. The relatively low conductivity of the studied TPMs necessitates such a massive amount of inactive components in the electrodes (usually 50 wt %^[8a,11,12,15a,16] or even higher^[17]). Besides, most of these prior studies used multistep synthesis procedures to develop functionalized TPMs (e.g., Figure S1a). This increases cost and often leads to poor yields, thereby making it challenging to use those materials in practical applications. To bring the TPMs to a practical level, both a higher active material ratio in the electrode and low-cost active material synthesis procedure are needed.

To achieve this, we demonstrate that a rational design of the substituents on the π -ring system can improve the electrical conductivity and cycling stability of TPMs and enhance their potential for practical applications. The utilized (4-aminophenyl)-porphyrins (xTAPP) in this study were synthesized with more than 74% yield^[18] in a single-step procedure (Figure S1b). This is a significant advantage over previously reported porphyrin electrode materials, such as CuDEPP, which required multiple synthesis steps and thus incurred higher production costs. A combined theoretical and experimental study was performed to determine the desired metal ion to centrally coordinate TAPP. Interestingly, metal-TAPPs could polymerize into a highly crosslinked conjugated network without the need for additional linking groups and pre-polymerization step. Thus, high capacity is achieved at less synthesis effort, and improved cycling stability is attained. Most importantly, the enhanced electrical conductivity reduces the necessary amount of conductive carbon (as low as 5 wt %). Besides, aqueous processing was adopted to develop the electrodes to avoid toxic organic solvents and costly electrode processing procedures. All these findings result in a more sustainable way of energy storage and hold the potential for practical storage applications.

Results and Discussion

Metal-free porphyrins are highly soluble in polar organic solvents and, therefore, rarely utilized as electrode materials in rechargeable energy storage systems.^[19] Even for porphyrins with limited solubility, the dissolution of the oxidized (16 π -

electrons system) and reduced (20 π -electrons system) forms will still impair its practical application (Figure 1a). This dissolution issue might be also a reason for the notable decline in the discharge capacity of bare metal-free porphyrins^[10] including tetraminophenyl-porphyrins (Figure 1b). There are several possibilities to effectively suppress the undesired solubility and improve the performance of the porphyrin electrodes. A commonly utilized approach in this respect is the implementation of central metal atoms into the porphyrin structure. The criteria for battery application are that the bonding between the central metal atom and porphyrin must be stable in the selected voltage window. Furthermore, the metal ions should ideally fit into the square planar cavity formed by the four pyrrole nitrogen atoms of porphyrins. Besides, the degree of the complex planarity will directly affect the packing and solubility of the metal-porphyrin electrodes.

Density functional theory (DFT) computations were performed to reveal the consequence of the central metal on the molecular geometries and electronic properties of metal-TAPPs. The frontier orbitals (FOs) of Zn- and Cu-complexes are mainly distributed on the porphyrin skeleton, while the FOs of NiTAPP showed substantial contribution from the Ni center (Figure S2). Energetically, the HOMO and LUMO of Zn- and Cu-complexes are hardly affected with respect to the TAPP reference (Figure S3). In the DFT-optimized geometries, the Ni-complex appears to undergo saddling distortions (Figure 1d). In contrast, the Cu- and Zn-complexes show a nearly planar structure in their DFT-optimized geometries (Figure 1e and f, Figure S4). The results obtained are in excellent agreement with UV-Vis absorption spectroscopy (Figure S5). The spectrum of pristine TAPP consists of a strong Soret band and four weak Q bands. Introduction of the central metal and the resulting changes in the symmetry are expected to strongly affect the wavelengths and intensities of the Q bands in the electrolyte and, consequently, significant decline in the capacity of the NiTAPP (Figure S6).

The planar complexes of TAPPs were further investigated in this study. Figure 2(a) shows the corresponding charge discharge curves of CuTAPP while cycling with a current density of 1 A/g. The first cycle displays high overpotential during charging, which could be attributed to an in-situ electro-polymerization during the oxidation. In addition, a relatively high discharge capacity of 149 mAh/g was obtained in the first cycle. In the following cycles, the capacity stabilized in the range between 119 mAh/g (50th cycle) and 114 mAh/g (1000th cycle). Interestingly, 96 of this capacity was retained after 1000 cycles at a high current density of 1 A/g. Even after 2000 cycles the capacity retention was 85%. This underlines the excellent cycling stability of the material.

The contribution of conductive carbon to the capacity is in general negligible (Figure S7) and no porphyrin cathodes containing 70 wt % of active material have been reported with such high capacities so far, to the best of our knowledge. Until now, research on TAPP for batteries, was done by Han *et al.*,^[20] who reported on a pre-polymerized aminophenyl-porphyrin complex which was utilized as an anode material and displayed high specific discharge capacities of up to 650 mAh/g at

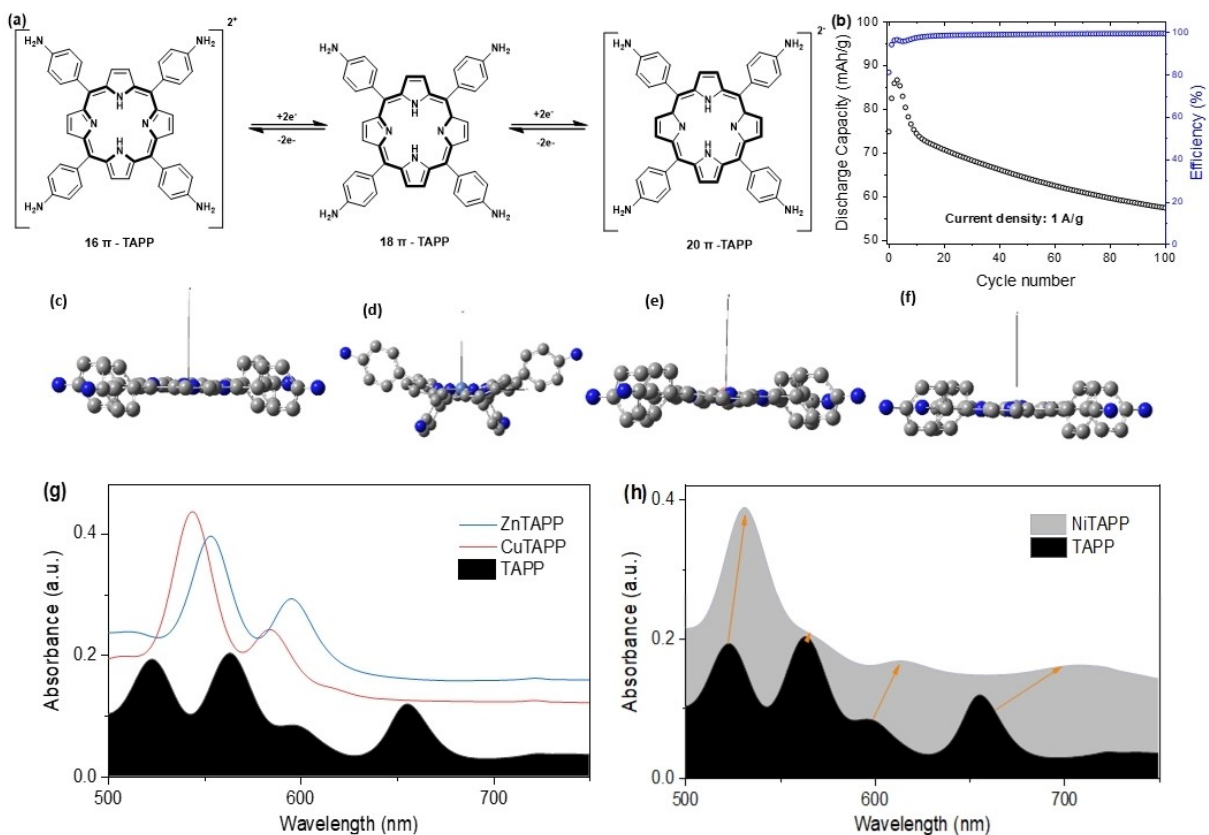


Figure 1. a) Two electron oxidation and two-electron reduction reactions of TAPP and b) its cycling performance in a Li half-cell with LiPF_6 based electrolyte in the potential window of 1.8–4.5 V. DFT-optimized structures of c) TAPP, d) NiTAPP with saddled distortion, as well as e) CuTAPP and f) ZnTAPP with almost planar core. Q-band region in UV-VIS absorption spectra of g) the planar metal-TAPPs and h) saddled NiTAPP.

100 mA/g. The polymers were assembled into nanosheets in an aqueous solution which improved the bulk conductivity at room temperature. Furthermore, Cu-tetraaminephthalocyanine, which is a distant derivative of CuTAPP, was successfully tested in dual-ion batteries with a high reversible capacity of 74.3 mAh/g after 4000 cycles at a current density of 4 A/g.^[8b] Therefore, the utilization of CuTAPP might be beneficial for increasing the energy density of the material and thus open the possibility of commercial cells with a high amount of porphyrin active material.

When comparing the cycling performance of the metal porphyrins (Cu- and ZnTAPP) to pristine TAPP (Figure 2c), a significant improvement was observed by introducing copper or zinc into the structure. The maximum discharge capacity of ZnTAPP (101 mAh/g) (Figure S8) and especially CuTAPP (149 mAh/g) exceeded the one of TAPP (86 mAh/g). Moreover, for TAPP the decay of discharge capacity was more substantial, and the capacity dropped by 53% within the first 500 cycles. The metallated porphyrin electrode materials did not only display higher initial capacities but also better cycling stability as maximum capacity retention after 2000 cycles was roughly 85% for CuTAPP and 70% for ZnTAPP. The remarkable performance of CuTAPP could be due to changes in the chemical structure which are discussed in detail in a following section.

The rate capability of xTAPPs was examined at current densities between 0.2 and 8 A/g (Figure 2d). The corresponding charge-discharge profiles are presented in Figures 2b and S9. The incorporation of Zn(II) and Cu(II) metal atoms greatly improves the discharge capacity and rate capability of TAPP. This could be attributed to the changes in the physical properties of the porphyrin material,^[21] including solubility, molecule planarity and crystallinity, which will be further explored in the study. At 0.2 A/g the achieved discharge capacity of CuTAPP was around 130 mAh/g in the 2nd cycle and was well above the ones from ZnTAPP (~120 mAh/g) and TAPP (~75 mAh/g). Even at a current density of 8 A/g, CuTAPP delivered a discharge capacity of around 60 mAh/g, whereas the values for ZnTAPP (36 mAh/g) and TAPP (6 mAh/g) were substantially lower. When returning to a current density of 0.2 A/g, metallated TAPPs almost restored the initial capacity values. As an example, the regained capacity was 128 mAh/g for CuTAPP after 120 cycles, demonstrating a good stability. This indicates that metallated TAPP structures are retained upon cycling at various rates and are probably not affected by parasitic reactions or strong solubility.

A detailed kinetic analysis (Figures S12–S15) was carried out to gain more insight into the influence of the central metal on the energy storage mechanism. The CVs (Figure S12c–e) of the metallated porphyrins CuTAPP and ZnTAPP show stronger

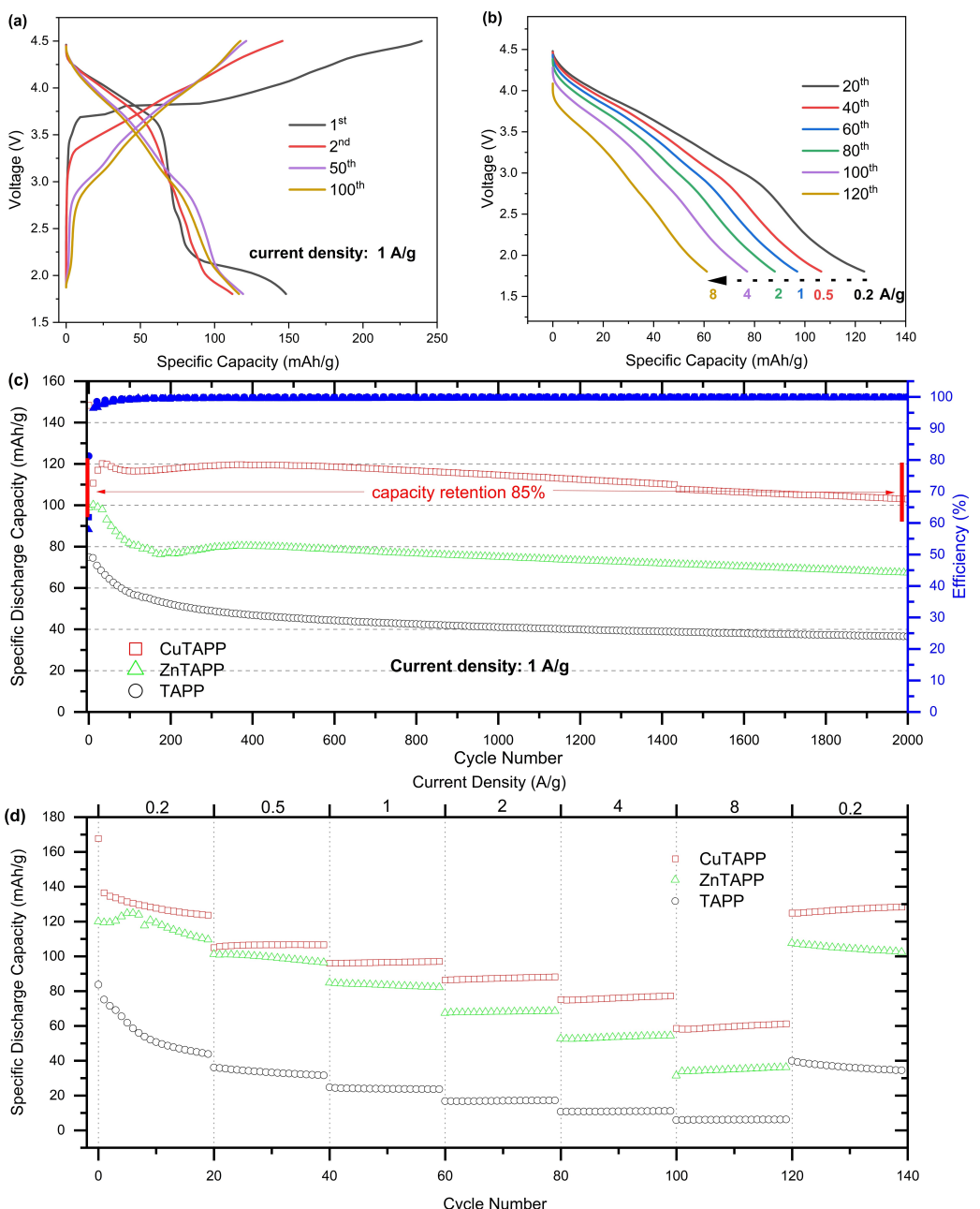


Figure 2. Selected charge-discharge profiles of CuTAPP a) at a current density 1 A/g and b) at differing current densities in the range between 0.2 to 8 A/g. c) The corresponding cycling performance and d) rate capability test of CuTAPP are compared to TAPP and ZnTAPP.

capacitive character than that of TAPP, which might explain their improved rate capability. These findings are supported when calculating the contributions of surface and diffusion controlled cycling reactions by applying an equation

$(i_v = k_1 v + k_2 v^2)$ proposed by Wang *et al.*^[22] (Figures S13–S15). At lower scan rates, both charge storage processes, surface and diffusion-dominated, were present with significant contributions for all xTAPPs. The contribution from the surface-controlled reaction increased with increasing scan rate up to 94% and 91% for CuTAPP and ZnTAPP, respectively, at 10 mV/s. For the pristine TAPP material, this value was only

81%, revealing a stronger battery-type material character than the metallated derivatives. In total, these results indicate effective surface charge storage of aminophenyl-porphyrin compounds and show their pseudocapacitive properties.

Organic electrodes exhibit low conductivity, which is often compensated by either a low active material content or a low electrode loading. For CuTAPP, on the contrary, we produced electrodes with 70 wt % active material content and a loading between 1.5–3.5 mg/cm². Comparing the stabilized energy density of CuTAPP electrodes to other organic cathode materials, including porphyrins,^[8a,10] a superiority of CuTAPP is obvious (Figure 3). In general, copper porphyrin active materials

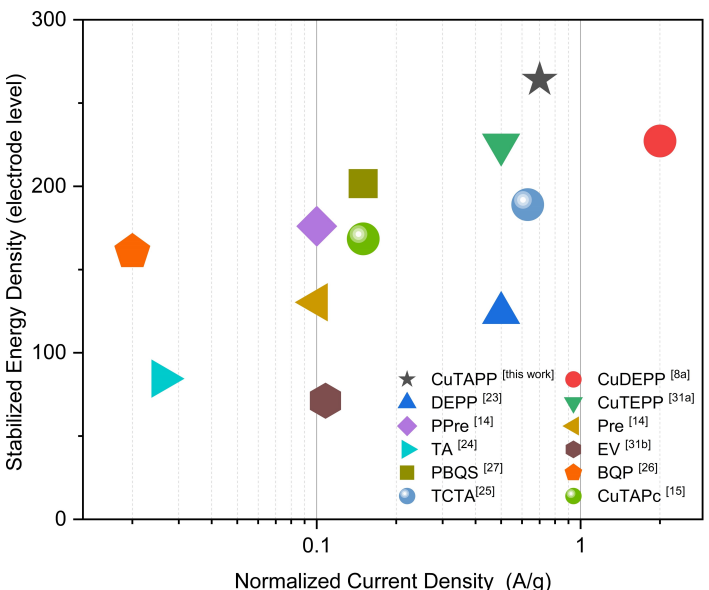


Figure 3. Comparison of different organic cathode materials in lithium cells with regard to their energy density based on the electrode loading. The energy density (after 200 charged cycles) is given as a function of the normalized current density (multiplied with the active material content) and was derived from various sources.^[8a,14,15,23–27,31]

(CuTAPP, CuDEPP,^[8a] and CuTEPP^[23]) show the highest stabilized energy densities (energy density after 200 cycles), making them promising for high performance energy storage. This result is based on two factors:

1. the improved charge storage of b-type materials enables high storage capacities due to multielectron redox and
2. the introduction of copper metal centers substantially improves the structural stability and electrochemical performance.^[10]

Additionally, the fact that porphyrins were charged with highest current densities and delivered the highest energy densities underlines their excellent rate capability behavior. In comparison, n-type organic materials (e.g., tannic acid (TA)^[24]) are limited by low voltages, whereas p-type materials (e.g., 4,4',4''-Tris(carbazol-9-yl)-triphenylamine (TCTA)^[25]) were not able to achieve similar storage capacities. Even stable polymeric electrodes (poly[5,15-bis(2,6-di-octoxyphenyl)-10,20-bis(ethynyl)-porphinato]zinc(ii) (PPre),^[14] benzoquinone polymer (BQP),^[26] or poly(benzoquinonyl sulfide (PBQS)^[27]) were not able to compete with copper porphyrin materials when comparing the energy density.

In commercial LIBs, the percentage of conductive carbons can be below 10 wt%^[28] because the electrode material often possesses a certain intrinsic conductivity. However, this is very challenging with organics as their electronic conductivity is limited. In an earlier study for porphyrin electrode materials,^[10] a fast capacity decay in the initial cycles was reported when increasing the amount of porphyrin active material to 80 wt%. Interestingly, CuTAPP did not show such a behavior, underlining again that less conductive agent is needed. Surprisingly, even with 5 wt% of conductive carbon additive, CuTAPP achieved outstanding cycling performance and reached maximal discharge capacities above 88 mAh/g (Figure S10). Upon

20 cycles of activation, the capacity gradually increased and more than 96% of the capacity was retained after 150 cycles. Then, the charge-discharge profiles resembled strongly the previous results with lower active material content and the coulombic efficiency was above 95%. This finding is especially important in practical application of organic electrodes for energy storage. In addition, it was found that such electrodes are also universal and could be used in diverse metal-based^[29] or metal-free^[30] storage systems. Our initial evaluation of the CuTAPP in a sodium half-cell indicated a similar performance to the Li-based cell (Figure S11). Typically, upon cycling a current density of 100 mA/g, CuTAPP reached a discharge capacity of 132 mAh/g after 10 cycles.

Further evaluation also revealed that the thermal stability of the developed porphyrin-based active materials was equal to or exceeded that of most organic electrode materials such as the quinones-materials^[32] or other organic materials.^[33] Thermogravimetric analysis with integrated differential scanning calorimetry (TGA-DSC) results (Figure S16) showed that decomposition of pristine TAPP started at above 150 °C with a 5% weight loss at a temperature ($T_{(5)}$) of around 265 °C, with no preceding phase change. Obviously, the introduction of the central metal greatly stabilizes the system leading to considerably improved thermal stabilities, with the $T_{(5)}$ rising to above 300 °C. Remarkably, Zn and Cu complexes retained above 70 wt% at 800 °C. This high thermal stability and the fact that xTAPPs are oxygen-free cathodes are critical features to ensure the safe operation of the storage system^[34] and its possible operation at elevated temperatures.^[35]

For a deeper understanding of the charge storage mechanism, cyclic voltammetry (CV) measurements were carried out with xTAPP electrodes at a scan rate of 1 mV/s. The voltage range during testing was between 1.8 V and 4.5 V and was

chosen based on the stability of the electrolyte (4.5 V) and the metal porphyrin (1.8 V). For CuTAPP four reduction peaks at 3.9 V, 3.5 V, 2.6 V and 2.3 V were detected, which could be attributed to the redox reaction from the dicationic to the dianionic form^[7a,8a] (Figure 4b). During the anodic sweep, the CV shows two peaks at 3.5 and 3.9 V.

For CuTAPP, a large irreversible peak in the CV at 3.9 V and an overpotential in the charge-discharge profiles were observed in the first oxidation sweep (Figure 4b). From the literature,^[36] it is known that tetraaminophenyl-porphyrins are able to undergo a polymerization reaction by forming a dihydrophenazine bond to build larger networks (Figure 4a). So far, the polymerization of aminophenyl-porphyrins was either performed by *ex-situ* pre-polymerization using Fe^{3+} -ions as reacting agent^[20] or *in-situ*, where the porphyrin monomers

were dissolved in the electrolyte and then immobilized during the cycling process on an electrode surface.^[36c] Despite the simplicity of the second pathway, it just leads to thin films of polymers and is rather impractical for large scale energy applications like batteries. That is why in our approach the aminophenyl-porphyrins were directly coated on the electrodes surface and underwent electropolymerization during the first cycle. The polymerization within the first oxidation step was beneficial to reduce the solubility of porphyrin molecules in the solvent and to improve the conductivity. This feature was also observed for TAPP and ZnTAPP, although the position of the peak shifted to 3.5 V and 4.3 V, respectively (Figure S12a and b).

For proving the successful *in-situ* electropolymerization, ex-situ FT-IR spectra were collected from pristine, charged and

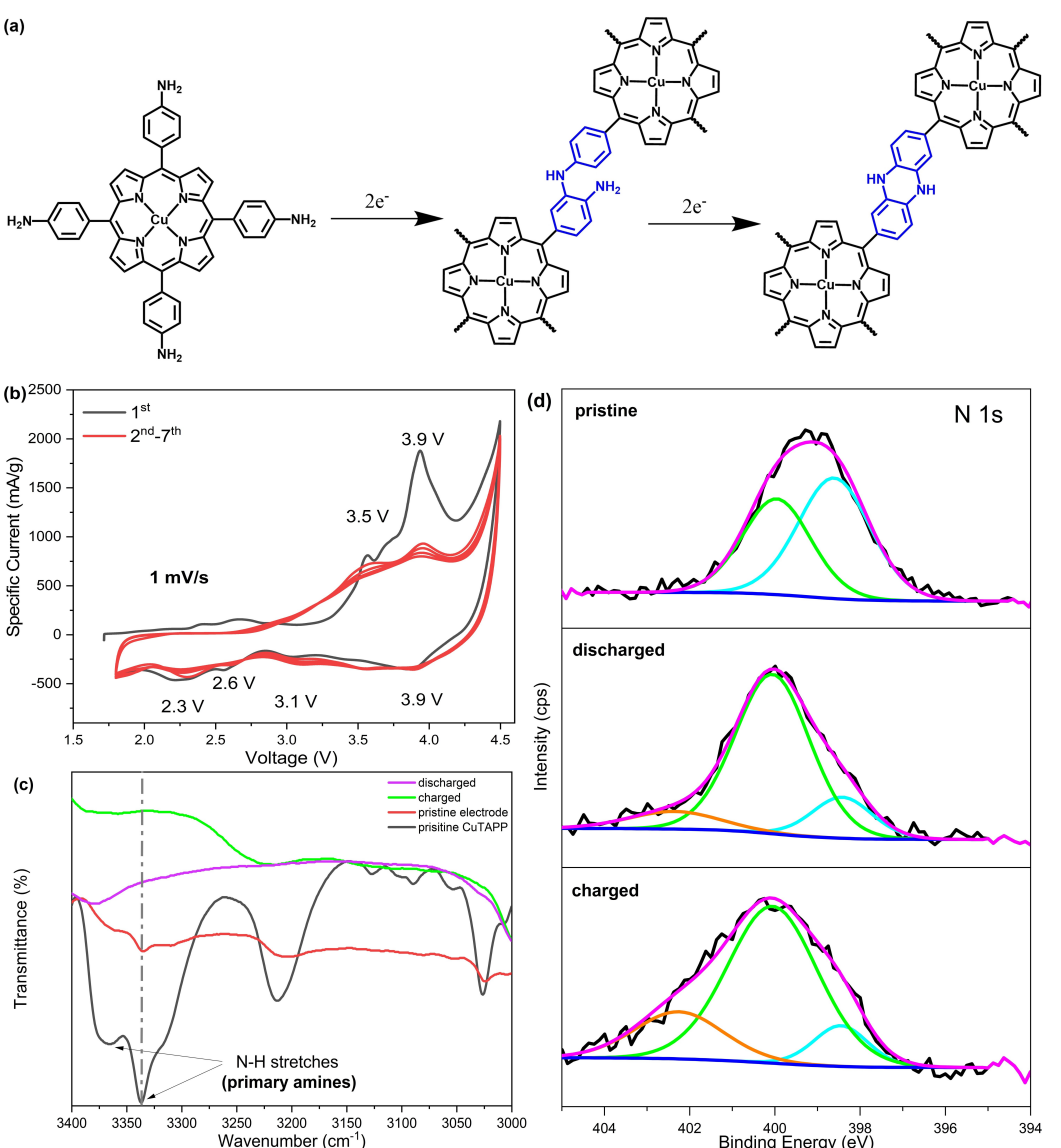


Figure 4. a) The schematic illustration of the *in-situ* electropolymerization mechanism of CuTAPP. The electropolymerization was investigated by b) cyclic voltammetry and c) proved by comparing the infrared (IR) spectra of the pristine powder (black), pristine electrode (red), and the electrodes in the charged (green) and discharged (violet) states between 3400 cm^{-1} and 3100 cm^{-1} . d) XPS detail spectra in the N1s region of CuTAPP electrodes in the pristine, charged (at 4.5 V) and discharged (at 1.8 V) state.

discharged CuTAPP electrodes (Figures 4c and S20). The peak at 3334 cm^{-1} , which is assigned to the stretch of the N–H group, can be well observed for both, the pristine powder and also the pristine CuTAPP electrode (Figure 4c). This band clearly disappears in the charged and discharged electrodes. Also, the other vibrational bands, namely N–H bending and N–H wagging, progressively disappear (Figure S20b and c). In contrast, the formation of the N–H wagging bond of secondary amines was observed for the cycled electrodes (Figure S20), which corroborates the polymerization reaction towards dihydrophenazine. The polymerization up to the phenazine bond, as described in literature,^[20,36] could not be observed even after charging the electrode for 1000 cycles (Figure S21). SEM-EDX (Figure S18) and ex-situ FTIR (Figure S21) of cycled CuTAPP electrodes rather show that the porphyrin material is stable upon cycling. Therefore, regardless of the electropolymerization in the first cycle, the appearing redox reactions are reversible and the structure of the molecule is retained.

For more insights into the charge storage mechanism of aminophenyl-porphyrin compounds, ex-situ XPS measurements were performed. In the N1s detail spectra (Figure 4d), two major changes are observable when comparing the results of cycled samples to the pristine one. First the peak intensity at 400.2 eV is increased which could correspond to the formation of dihydrophenazine functional groups.^[37] The second feature at 402.5 eV is well known in literature^[25,38] and is assigned to the assembly of N-PF₆⁻ interactions, which are formed during the charging of porphyrins.

Also, when examining the Cu 2p core spectrum of the cycled electrodes via XPS (Figure 5a), the data of the discharged sample shows a splitting of the copper peaks into two contributions. This indicates a reduction reaction and therefore the change from Cu(II) to Cu(I) seems plausible although the reduction of Cu-centers occurs just partially. A substantial contribution for the increased capacities of CuTAPP electrodes might come from this additional redox reaction happening at the metal center and could be a possible reason for the improved electrochemical properties. In contrast, the Zn 2p spectrum (Figure 5b) of ZnTAPP does not show the occurrence of another peak and is accordingly also not reduced in the discharge step.

To further investigate the reason behind the improved cycling behavior of CuTAPP, the structure and morphology of this material was investigated and compared to the other xTAPPs. TAPP and ZnTAPP consisted of mostly round particles with fairly distributed sizes. The particle size of all xTAPPS was in the same range roughly between 1–10 μm . In contrast, the SEM of CuTAPP showed stacked-sheet-like structures (Figures 6b and S17) with irregular particle sizes and forms. Interestingly, these irregular particles were highly crystalline as shown in the powder XRD (Figure 6a). CuTAPP shows sharp reflections with relatively good signal to noise ratio. In contrast, the pattern of ZnTAPP and TAPP showed significant amorphization, as many of the detected peaks were widely broadened over several degrees. We expect that the highly crystalline nature of CuTAPP results from the molecular stacking of

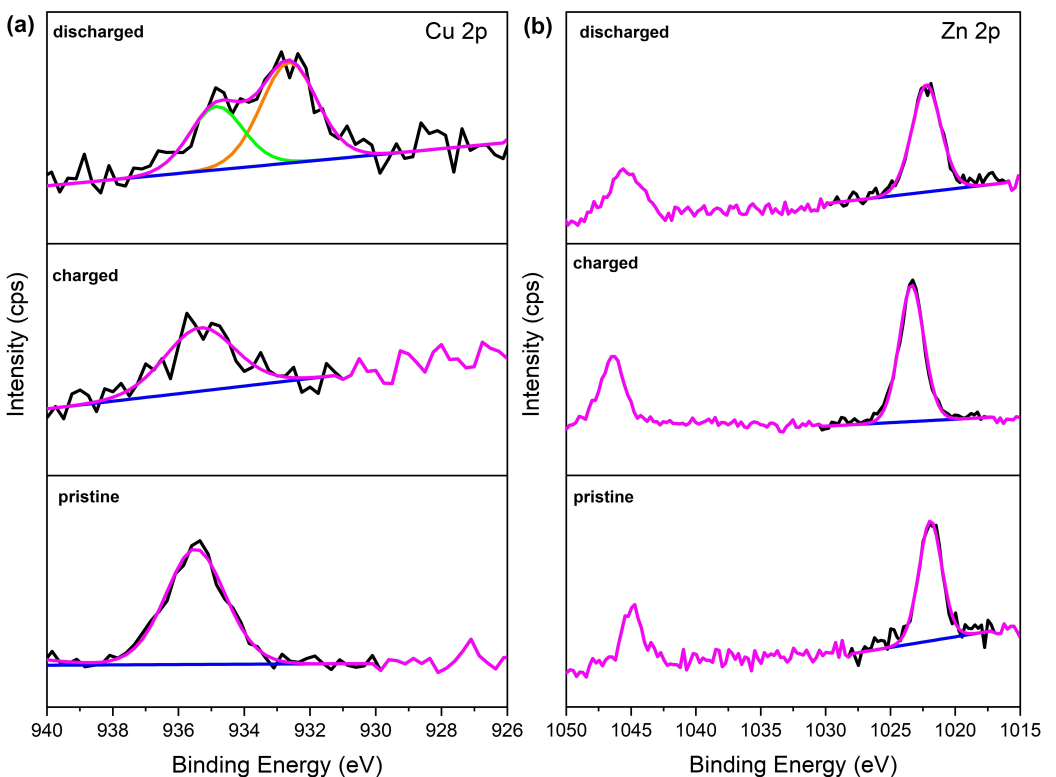


Figure 5. a) XPS detail spectra in Cu 2p region of CuTAPP in the pristine, charged (at 4.5 V) and discharged (at 1.8 V) states show the formation of Cu(I) in the discharge. b) This behavior is not observed for ZnTAPP in the XPS detail spectra in the Zn 2p region of pristine, charged (at 4.5 V) and discharged (at 1.8 V) states.

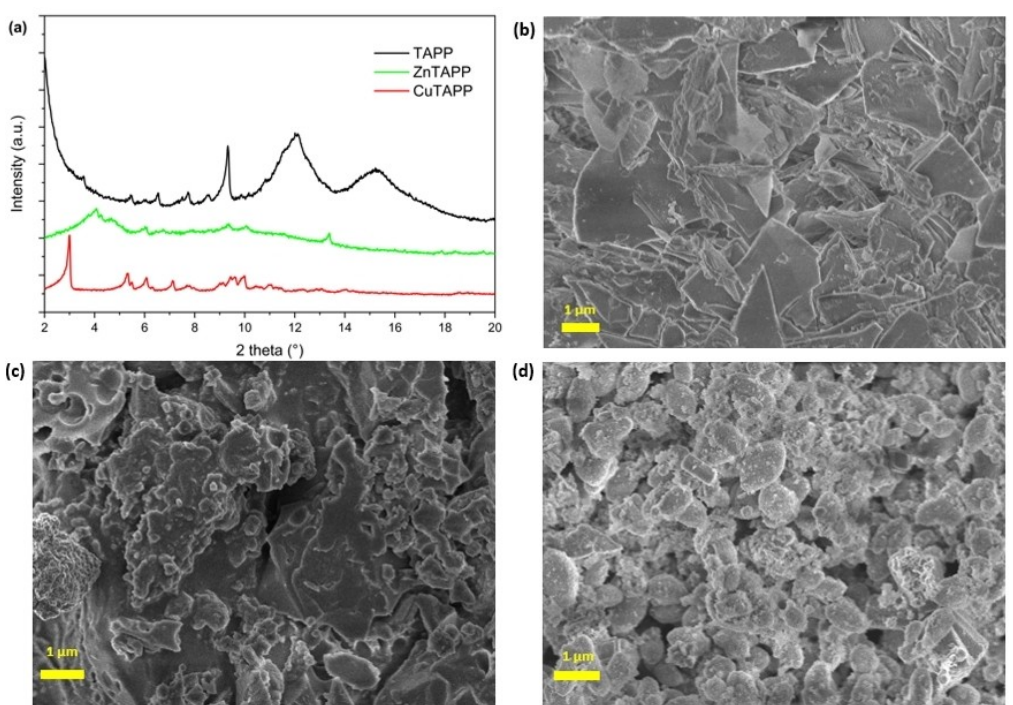


Figure 6. Crystallinity was examined via a) powder XRD for TAPP (black), ZnTAPP (blue) and CuTAPP (red) in the range between 2° and 20° (2 theta). Morphology of b) pristine CuTAPP, c) TAPP and d) ZnTAPP studied via SEM.

porphyrins. This molecular stacking could play an important role for the electrochemical properties and be the reason behind enhanced cycling stability and/or rate capability as shown in Figure 2 (c and d), respectively. It was shown before that the stacking of the molecules in the electrode might influence the energy barrier for electron transfer between neighboring molecules, and therefore change the intrinsic conductivity of the material.^[39] The enhancement of conductivity in the CuTAPP electrode was confirmed by comparing its through-plane conductivity measurements (as seen in Figure S25) to those of the metal-free porphyrin, which revealed a higher conductivity in the CuTAPP electrode. This improvement

in conductivity can be attributed to the efficient stacking of its molecules. Impedance measurements also showed an enhancement of the charge-transfer in CuTAPP when compared to the other xTAPPs (Figure 7a). Due to the ordered sheet-like structure, the Li-ion diffusion pathways might be shortened which could be beneficial for more efficient charge storage.^[40] Nevertheless, more research is needed to fully understand the impact of microstructure on the cycling behavior of such porphyrins.

The second aspect of these EIS-measurements can be found when comparing the initial Nyquist plot with the ones after the first cycle (Figure 7b). For all materials, the charge transfer

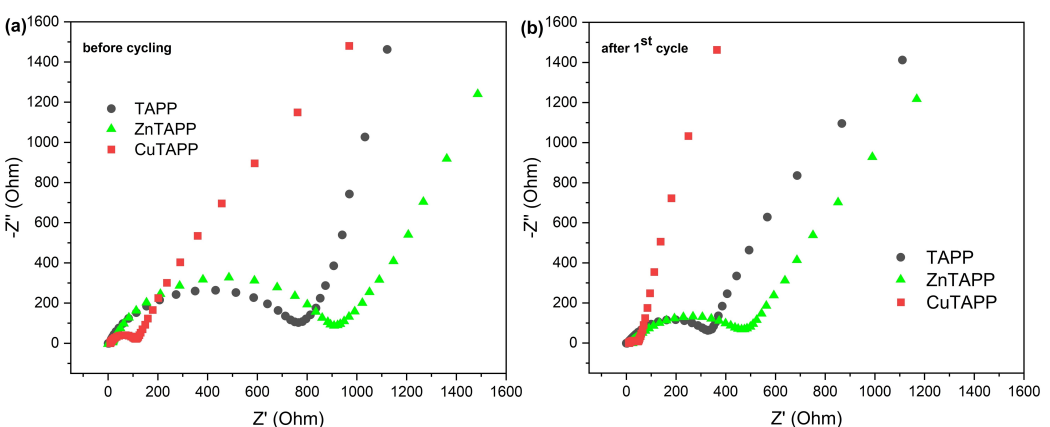


Figure 7. Nyquist plots for TAPP (black), ZnTAPP (green) and CuTAPP (red) a) before cycling and b) after the first cycle. The Nyquist plots were always recorded after an OCV-period lasting 2 hours.

resistance got reduced and was roughly halved. It seems that the electropolymerization is having a positive influence on the charge transfer resistivity. In the low frequency region, the slope of CuTAPP is higher than the one of the two other porphyrins. This shows that the diffusive resistivity in polymerized CuTAPP is lower and that ions can be accommodated in the electrode more quickly.^[20,41] This would also explain the improved rate capability of CuTAPP materials and point out the pseudocapacitive character of porphyrin again.

Conclusion

In conclusion, we were able to demonstrate that porphyrins with specific functionalities can enhance their potential for practical applications through specific measures. Specifically, it was shown for the first time that the 4-aminophenyl substituent on the π -ring system enabled *in-situ* electropolymerization of the active materials during the cycling leading to more stable performance and higher conductivity simultaneously. The performance of this relatively low-cost and easy to synthesize aminophenyl-porphyrins (with over 74% yield in a single-step procedure) could be further improved by introducing Cu^{2+} as the central metal, which was found to be redox active during the cycling itself thereby contributing to higher performance of the active material.

Despite the redox activity of the central metal and the *in-situ* electropolymerization in the initial cycles, the polymerized cathode is stable during extended charge/discharge cycling in Li- and Na-based systems, which is also an essential requirement for considering further practical applications with porphyrins and organic electrodes in general.

These features clearly illustrate the potential of metalloporphyrins for practical organic electrodes and pave the way for developing new sustainable electrochemical energy storage systems.

Experimental

Materials. Aminophenyl-porphyrin derivatives were obtained commercially (TAPP: PorphyChem SAS, France-; ZnTAPP, NiTAPP and CuTAPP: Por-Lab Porphyrin-Laboratories GmbH; Germany) and were used without any further purification. Conductive carbon (Super P, Alfa Aesar, 99 + % on metal basis) was dried for 12 h at 300 °C in vacuum (1×10^{-3} mbar). Also, the binders, namely sodium-carboxymethyl cellulose (CMC, Sigma Aldrich; $M_w \approx 250$ kDa) and styrene-butadiene copolymer rubber (SBR, MTI Corporation), were purchased. Glass microfiber separators (Whatman, GF/C) were dried at around 200 °C in vacuum over 12 hours.

Electrode preparation. The electrode slurry was prepared by mixing the aminophenyl-porphyrin active materials with Super P conductive carbon, carboxymethylcellulose and styrene-butadiene rubber in a respective ratio of 7:2:0.6:0.4 in water. The mixing was performed in a planetary centrifugal mixer (Thinky ARE-250) for 20 minutes at 2000 rpm. The slurry was blade-casted on carbon-coated aluminum foil with a wet-film thickness of 150 μm and pre-dried in air atmosphere at ambient temperature overnight. Electrode discs of 11.8 mm diameter were cut out the casted foil

and were dried in high vacuum at 80 °C for 12 hours. After drying, the electrode discs with a total mass loading between 1.5 to 3.5 mg/cm² were transferred and stored in an Argon-filled glove box.

Electrochemical cell tests. Electrochemical cell tests of cyclic voltammetry, charge-discharge cycling and rate capability tests were performed on a Biologic VMP-3 potentiostat and on a Biologic BCS 805 battery testing unit. The applied voltage window was between 1.8–4.5 V against Li. The CV measurements were performed with different scan rates from 0.1 to 10 mV/s. The coin-cell assembly was conducted in an argon-filled glovebox. For testing the electrochemical performance, CR2032 coin cells were built with Li and Na metal and glass microfibers (GF/C) separators. The electrolyte was 1 M LiPF₆ as salt inside a mixture of ethylene carbonate (EC), propylene carbonate (PC) and dimethyl carbonate (DMC) in a volume ratio of 1:1:3 (V(EC):V(PC):V(DMC)) for lithium ion cells and 1 M NaPF₆ in ethylene glycol dimethyl ether (DME) for sodium ion cells. Electrochemical impedance spectroscopy (EIS) was performed in a Swagelok cell setup using AC-frequencies between 50 mHz and 1 MHz. The measurement was always performed after a 2 h OCV-period to minimize polarization effects.

Structural and chemical characterization. SEM measurements were performed to study the morphology of the materials, using a Zeiss Leo Gemini 1530 System. For the investigation of the crystallinity, powder XRDs were measured on a Stoe Stadi P with monochromatic Mo K_{α1} radiation ($\lambda = 0.07093$ nm). The applied operational current and voltage were 50 mA and 40 kV, respectively. The chemical state was studied by X-ray photoelectron spectroscopy (XPS) measurements in a Specs XPS system with a Phoibos 150 energy analyzer. The measurements were acquired using monochromatic Al K_α radiation (1486.6 eV), a take-off angle of 45° and pass energies of 30 and 90 eV at the analyzer for detail and survey spectra, respectively. For binding energy calibration, the C1s main peak was set to 284.8 eV. Peak fitting was carried out with CasaXPS software with Shirley-type backgrounds and Gaussian-Lorentzian peak profiles. FT-IR spectra were collected on a Perkin Elmer FT IR Spectrum Two unit in the ATR-mode. The scanning range was between 4000 cm⁻¹ and 400 cm⁻¹. For the ex-situ studies, IR measurements were done inside an Ar-filled glovebox. Liquid NMR measurements were performed on a Bruker DRX 500 (500 MHz frequency). For the measurement the porphyrins were dissolved in deuterated DMSO-d6. Thermal stability was examined by using TGA-DSC analysis using a Setaram Sensys Evo TG-DSC machine. The analysis was done under permanent Ar-flow (20 mL/min) and a heating rate of 5 °C/min. UV-VIS measurements were performed on a Varian Cary 5000 UV-VIS/NIR spectrophotometer.

Acknowledgement

This work contributes to the research performed at CELEST (Center for Electrochemical Energy Storage Ulm-Karlsruhe) and was funded by the German Research Foundation (DFG) under Project ID 390874152 (POLiS Cluster of Excellence, EXC 2154). We would like to express our appreciation to Mr. Jonas Mohacsi (KIT-Institute of Thermal Process Engineering-Thin Film Technology) for his invaluable assistance in the conductivity measurements of the electrodes. Open Access funding enabled and organized by Projekt DEAL.

Conflict of Interest

The authors declare no conflict of interest.

Data Availability Statement

The data that support the findings of this study are available from the corresponding author upon reasonable request.

Keywords: cathode materials · high active material content · in-situ electropolymerization · metal porphyrins · organic electrodes

- [1] a) P. Poizot, J. Gaubicher, S. Renault, L. Dubois, Y. Liang, Y. Yao, *Chem. Rev.* **2020**, *120*, 6490; b) A. Banerjee, N. Khosossi, W. Luo, R. Ahuja, *J. Mater. Chem. A* **2022**, *10*, 15215; c) H. Nishide, *Green Chem.* **2022**, *24*, 4650.
- [2] D. L. Thompson, J. M. Hartley, S. M. Lambert, M. Shiref, G. D. J. Harper, E. Kendrick, P. Anderson, K. S. Ryder, L. Gaines, A. P. Abbott, *Green Chem.* **2020**, *22*, 7585.
- [3] a) H. Zhang, Y. Gao, X. H. Liu, Z. Yang, X. X. He, L. Li, Y. Qiao, W. H. Chen, R. H. Zeng, Y. Wang, *Adv. Funct. Mater.* **2022**, *32*, 2107718; b) C. Ding, C. Li, H. Tian, Y. Tong, W. Huang, Q. Zhang, *Batteries & Supercaps* **2022**, *5*, e202200160.
- [4] J. Heiska, M. Nisula, M. Karppinen, *J. Mater. Chem. A* **2019**, *7*, 18735.
- [5] a) Z. Song, H. Zhou, *Energy Environ. Sci.* **2013**, *6*, 2280; b) B. Häupler, A. Wild, U. S. Schubert, *Adv. Energy Mater.* **2015**, *5*, 1402034.
- [6] J. Y. Shin, T. Yamada, H. Yoshikawa, K. Awaga, H. Shinokubo, *Angew. Chem.* **2014**, *126*, 3160.
- [7] a) Z. Zhao-Karger, P. Gao, T. Ebert, S. Klyatskaya, Z. Chen, M. Ruben, M. Fichtner, *Adv. Mater.* **2019**, *31*, 1806599; b) C. Luo, O. Borodin, X. Ji, S. Hou, K. J. Gaskell, X. Fan, J. Chen, T. Deng, R. Wang, J. Jiang, *Proc. Natl. Acad. Sci. USA* **2018**, *115*, 2004; c) Y. Zhang, L. Cheng, L. Zhang, D. Yang, C. Du, L. Wan, J. Chen, M. Xie, *J. Energy Storage* **2021**, *34*, 102018; d) T. Ma, Z. Pan, L. Miao, C. Chen, M. Han, Z. Shang, J. Chen, *Angew. Chem.* **2018**, *130*, 3212.
- [8] a) P. Gao, Z. Chen, Z. Zhao-Karger, J. E. Mueller, C. Jung, S. Klyatskaya, T. Diemant, O. Fuhr, T. Jacob, R. J. Behm, *Angew. Chem.* **2017**, *129*, 10477; b) H. g. Wang, H. Wang, Z. Si, Q. Li, Q. Wu, Q. Shao, L. Wu, Y. Liu, Y. Wang, S. Song, *Angew. Chem.* **2019**, *131*, 10310.
- [9] T. Philipp, G. Neusser, E. Abouzari-Lotf, S. Shakouri, F. D. H. Wilke, M. Fichtner, M. Ruben, M. Mundszinger, J. Biskupek, U. Kaiser, P. Scheitenberger, M. Lindén, C. Kranz, *J. Power Sources* **2022**, *522*, 231002.
- [10] X. Chen, X. Feng, B. Ren, L. Jiang, H. Shu, X. Yang, Z. Chen, X. Sun, E. Liu, P. Gao, *Nano-Micro Lett.* **2021**, *13*, 1.
- [11] S. Lv, J. Yuan, Z. Chen, P. Gao, H. Shu, X. Yang, E. Liu, S. Tan, M. Ruben, Z. Zhao-Karger, M. Fichtner, *ChemSusChem* **2020**, *13*, 2286.
- [12] E. Abouzari-Lotf, R. Azmi, Z. Li, S. Shakouri, Z. Chen, Z. Zhao-Karger, S. Klyatskaya, J. Maibach, M. Ruben, M. Fichtner, *ChemSusChem* **2021**, *14*, 1840.
- [13] X. Han, S. Li, W.-L. Song, N. Chen, H. Chen, S. Huang, S. Jiao, *Adv. Energy Mater.* **2021**, *11*, 2101446.
- [14] J. Yuan, B. Ren, X. Feng, P. Gao, E. Liu, S. Tan, *Chem. Commun.* **2020**, *56*, 5437.
- [15] a) H.-g. Wang, H. Wang, Z. Si, Q. Li, Q. Wu, Q. Shao, L. Wu, Y. Liu, Y. Wang, S. Song, H. Zhang, *Angew. Chem. Int. Ed.* **2019**, *58*, 10204; b) P. Gao, *Novel electrode materials for rechargeable batteries based on cationic and anionic shuttles*, Universität Ulm, Ulm 2016.
- [16] a) Z. Chen, P. Gao, W. Wang, S. Klyatskaya, Z. Zhao-Karger, D. Wang, C. Kübel, O. Fuhr, M. Fichtner, M. Ruben, *ChemSusChem* **2019**, *12*, 3737; b) X.-M. Lin, D.-Y. Wu, P. Gao, Z. Chen, M. Ruben, M. Fichtner, *Chem. Mater.* **2019**, *31*, 3239; c) X. Judez, L. Qiao, M. Armand, H. Zhang, *ACS Appl. Energ. Mater.* **2019**, *2*, 4008.
- [17] L. Mei, J.-C. Wei, Q. Duan, *J. Mater. Sci. Mater. Electron.* **2021**, *32*, 24953.
- [18] E. H. Tawfik, A. A. Fadda, N. N. Soliman, L. Abou-Zeid, A. Negm, *J. Porphyrins Phthalocyanines* **2019**, *23*, 251.
- [19] Y. Sun, F. He, X. Huang, B. Ren, J. Peng, D. Chen, X. Hu, X. Sun, P. Gao, *Chem. Eng. J.* **2023**, *451*, 138734.
- [20] Z. Han, Y. Ai, X. Jiang, Y. You, F. Wei, H. Luo, J. Cui, Q. Bao, J. Fu, Q. He, *Chem. Eur. J.* **2020**, *26*, 10433.
- [21] S. Shakouri, E. Abouzari-Lotf, J. Chen, T. Diemant, S. Klyatskaya, F. D. Pammer, A. Mizuno, M. Fichtner, M. Ruben, *ChemSusChem* **2022**, e202202090.
- [22] J. Wang, J. Polleux, J. Lim, B. Dunn, *J. Phys. Chem. C* **2007**, *111*, 14925.
- [23] X. Feng, X. Chen, B. Ren, X. Wu, X. Huang, R. Ding, X. Sun, S. Tan, E. Liu, P. Gao, *ACS Appl. Mater. Interfaces* **2021**, *13*, 7178.
- [24] Z. Xu, H. Ye, H. Li, Y. Xu, C. Wang, J. Yin, H. Zhu, *ACS Omega* **2017**, *2*, 1273.
- [25] C. Zhao, Z. Chen, W. Wang, P. Xiong, B. Li, M. Li, J. Yang, Y. Xu, *Angew. Chem.* **2020**, *132*, 12090.
- [26] K. Pirnat, G. Mali, M. Gaberscek, R. Dominko, *J. Power Sources* **2016**, *315*, 169.
- [27] Z. Song, Y. Qian, T. Zhang, M. Otani, H. Zhou, *Adv. Sci.* **2015**, *2*, 1500124.
- [28] J. Li, J. Fleetwood, W. B. Hawley, W. Kays, *Chem. Rev.* **2022**, *122*, 903.
- [29] a) L. Fan, R. Ma, J. Wang, H. Yang, B. Lu, *Adv. Mater.* **2018**, *30*, 1805486; b) K. Holguin, M. Mohammadiroobbari, K. Qin, C. Luo, *J. Mater. Chem. A* **2021**, *9*, 19083; c) D. Xu, M. Liang, S. Qi, W. Sun, L.-P. Lv, F.-H. Du, B. Wang, S. Chen, Y. Wang, Y. Yu, *ACS Nano* **2021**, *15*, 47; d) J. Bitenc, N. Lindahl, A. Vizintin, M. E. Abdelhamid, R. Dominko, P. Johansson, *Energy Storage Mater.* **2020**, *24*, 379.
- [30] a) J. Xie, Z. Wang, Z. J. Xu, Q. Zhang, *Adv. Energy Mater.* **2018**, *8*, 1703509; b) N. Casado, D. Mantione, D. Shanmukaraj, D. Mecerreyes, *ChemSusChem* **2020**, *13*, 2464.
- [31] a) X. Feng, X. Wu, X. Chen, J. Yuan, S. Lv, B. Ren, X. Sun, E. Liu, S. Tan, P. Gao, *Energy Storage Mater.* **2021**, *42*, 454; b) M. Chen, L. Liu, P. Zhang, H. Chen, *RSC Adv.* **2021**, *11*, 24429.
- [32] a) B. Zhao, Y. Si, W. Guo, Y. Fu, *Adv. Funct. Mater.* **2022**, *32*, 2112225; b) J. Yang, P. Xiong, Y. Shi, P. Sun, Z. Wang, Z. Chen, Y. Xu, *Adv. Funct. Mater.* **2020**, *30*, 1909597; c) G. Yoo, S. Pyo, Y. J. Gong, J. Cho, H. Kim, Y. S. Kim, J. Yoo, *Cellulose* **2020**, *27*, 6707.
- [33] a) A. Vlad, J. Rolland, G. Hauffman, B. Ernould, J.-F. Gohy, *ChemSusChem* **2015**, *8*, 1692; b) R. Zeng, L. Xing, Y. Qiu, Y. Wang, W. Huang, W. Li, S. Yang, *Electrochim. Acta* **2014**, *146*, 447; c) J. Y. Zhang, L. B. Kong, L. Z. Zhan, J. Tang, H. Zhan, Y. H. Zhou, C. M. Zhan, *J. Power Sources* **2007**, *168*, 278.
- [34] Z. Li, M. Dadsetan, J. Gao, S. Zhang, L. Cai, A. Naseri, M. E. Jimenez-Castaneda, T. Filley, J. T. Miller, M. J. Thomson, V. G. Pol, *Adv. Energy Mater.* **2021**, *11*, 2101764.
- [35] B. E. Gurkan, Z. Qiang, Y.-M. Chen, Y. Zhu, B. D. Vogt, *J. Electrochem. Soc.* **2017**, *164*, H5093.
- [36] a) M. V. Tesakova, O. I. Koifman, V. I. Parfenyuk, *J. Porphyrins Phthalocyanines* **2018**, *22*, 632; b) M. V. Tesakova, A. S. Semeikin, V. I. Parfenyuk, *J. Porphyrins Phthalocyanines* **2016**, *20*, 793; c) M. Tesakova, V. Sheinin, V. Parfenyuk, *Russ. J. Phys. Chem. A* **2014**, *88*, 325.
- [37] W. Ma, L.-W. Luo, P. Dong, P. Zheng, X. Huang, C. Zhang, J.-X. Jiang, Y. Cao, *Adv. Funct. Mater.* **2021**, *31*, 2105027.
- [38] L. Fan, Q. Liu, Z. Xu, B. Lu, *ACS Energy Lett.* **2017**, *2*, 1614.
- [39] a) Y. Diao, K. M. Lenn, W.-Y. Lee, M. A. Blood-Forsythe, J. Xu, Y. Mao, Y. Kim, J. A. Reinschbach, S. Park, A. Aspuru-Guzik, *J. Am. Chem. Soc.* **2014**, *136*, 17046; b) H. Jiang, P. Hu, J. Ye, K. K. Zhang, Y. Long, W. Hu, C. Kloc, *J. Mater. Chem. C* **2018**, *6*, 1884; c) D. V. Konarev, M. A. Faraonov, M. S. Batov, M. G. Andronov, A. V. Kuzmin, S. S. Khasanov, A. Otsuka, H. Yamochi, H. Kitagawa, R. N. Lyubovskaya, *Dalton Trans.* **2020**, *49*, 16821.
- [40] Y. Zhao, L. Peng, B. Liu, G. Yu, *Nano Lett.* **2014**, *14*, 2849.
- [41] Y. Ai, Y. You, F. Wei, X. Jiang, Z. Han, J. Cui, H. Luo, Y. Li, Z. Xu, S. Xu, J. Yang, Q. Bao, C. Jing, J. Fu, J. Cheng, S. Liu, *Nano-Micro Lett.* **2020**, *12*, 31.

Manuscript received: January 23, 2023

Revised manuscript received: February 5, 2023

Version of record online: March 3, 2023